

Control of Wannier orbitals for generating entanglement of ultracold atoms in an optical lattice

Kensuke Inaba,^{1,3} Yuuki Tokunaga,^{2,3} Kiyoshi Tamaki,^{1,3} Kazuhiro Igeta,^{1,3} and Makoto Yamashita^{1,3}

¹ NTT Basic Research Laboratories, NTT Corporation, Atsugi 243-0198, Japan

² NTT Information Sharing Platform Laboratories, NTT Corporation, Musashino 180-8585, Japan

³ JST, CREST, Chiyoda-ku, Tokyo 102-0075, Japan

(Dated: June 3, 2019)

We propose a method for controlling the quantum state of ultracold atoms in an optical lattice by using current atom manipulation techniques, which can generate high-fidelity entanglement resources. We utilize higher Wannier orbitals as a *controllable and accessible* environment, and then realize a tunable Ising interaction between atoms in the lowest orbital to generate multipartite entangled cluster states. We can enhance the fidelity by employing a post-selection scheme based on spectroscopic measurements of states in the environment. Precise numerical simulations using realistic parameters suggest that our method offers significant advantages for high-fidelity entanglement generation toward scalable measurement-based quantum computation.

PACS numbers: 03.67.Lx, 03.67.Bg, 37.10.Jk, 71.10.Fd

Measurement-based quantum computation (MBQC) [1, 2] is a prominent method for scalable quantum information processing because we can perform a universal quantum computation with only successive single-qubit measurements after preparing large entangled resources, such as multipartite entangled cluster states. Ultracold atoms with pseudospin (*e.g.* hyperfine) states in an optical lattice are promising candidates with which to implement MBQC [3]. This clean and isolated system will sustain quantum coherence for a long time [3]. State-of-the-art experiments using coupling between lights and atoms demonstrate that a single atom can be detected and manipulated by addressing the lattice sites individually [4, 5], suggesting substantial progress on single-qubit measurement techniques. The other key issue, the multipartite entanglement generation, has been discussed in theoretical studies [6–9] and has also been demonstrated experimentally [10]. However, high fidelity and scalability, which are important features in the implementation of MBQC, have not been fully confirmed even theoretically. Especially, change of the atomic orbitals and multiple site-occupancies, which have not been sufficiently taken into account, would indeed cause non-negligible errors in scalable quantum computing.

In this paper, we propose to exploit Wannier orbitals as controllable quantum states for generating high-fidelity entangled cluster states of ultracold fermionic atoms in an optical lattice. To make this control precise, we treat Wannier orbitals in the *ab initio* manner. In our method, atoms in the lowest orbital are chosen as qubits, and the extra-Hilbert space that originates from higher orbitals serves as a *controllable and accessible* environment. By controlling the coupling between the qubits and the environment, we can design interactions among the qubits. Specifically, we create a *tunable* Ising interaction in adjacent sites to generate entangled cluster states. The fidelity can be enhanced by performing measurements on

states of the environment followed by post-selection depending on the resulting outcomes. Moreover, substantial advantages as regards scalability can be obtained by our pair-wise entanglement generation scheme. Precise numerical simulations involving an exact diagonalization confirm that a combination of the above tricks allows us to generate very high-fidelity entanglement with current experimental technologies. The present method is applicable to generating one, two, and three dimensional (1D, 2D, and 3D) cluster states, and thus is suitable for fault tolerant MBQC schemes [11–14].

We begin by explaining our system. We consider fermionic atoms with two spins in an optical lattice. The non-interacting Hamiltonian of the atoms is given by $\mathcal{H}_0 = -\sum_i \frac{\hbar^2 \nabla_i^2}{2M} + V_0[\cos(x_i/a) + \cos(y_i/a) + \cos(z_i/a)]$, where V_0 is the lattice depth, a is the lattice distance, and M is the mass of the atoms. We solve \mathcal{H}_0 numerically, and calculate the eigenvectors and their Fourier transformation, namely, Bloch and Wannier orbitals. These Wannier orbitals are used to derive the full Hamiltonian, $\mathcal{H} = \mathcal{H}_0 + \mathcal{H}_{\text{int}}$, in the second quantization framework. Here, \mathcal{H}_{int} is the contact interaction term given by $\frac{4\pi\hbar^2 a_S}{M} \sum_{i,j} \delta(\mathbf{r}_i - \mathbf{r}_j)$, where a_S is the scattering length. The second quantized expression of \mathcal{H} is the multiorbital Hubbard Hamiltonian written as $\mathcal{H} = \sum_{\langle ij \rangle} \sum_{\sigma\alpha} J_{\alpha\alpha} c_{i\sigma\alpha}^\dagger c_{j\sigma\alpha} + \sum_i \sum_{\sigma\alpha} \varepsilon_\alpha c_{i\sigma\alpha}^\dagger c_{i\sigma\alpha} + \sum_i \sum_{\alpha\beta} U_{\alpha\beta} (c_{i\uparrow\alpha}^\dagger c_{i\uparrow\alpha} c_{i\downarrow\beta}^\dagger c_{i\downarrow\beta} + c_{i\uparrow\alpha}^\dagger c_{i\uparrow\beta} c_{i\downarrow\beta}^\dagger c_{i\downarrow\alpha}) + H.c.$, where $c_{i\sigma\alpha}^\dagger$ ($c_{i\sigma\alpha}$) are the creation (annihilation) operator of a fermion with a spin σ ($=\uparrow, \downarrow$) and an orbital α ($=1, 2, \dots$) at the i th site, and the subscript $\langle ij \rangle$ means the summation over the nearest-neighbor sites. Parameters, on-site potentials ε_α , hopping matrices to adjacent sites $J_{\alpha\beta}$, and interaction strengths $U_{\alpha\beta}$, are determined by *ab initio* calculations. We note that inter-orbital hopping matrices vanish due to orthogonality of the set of the Bloch functions, *i.e.*, $J_{\alpha\neq\beta} = 0$. We assume that the

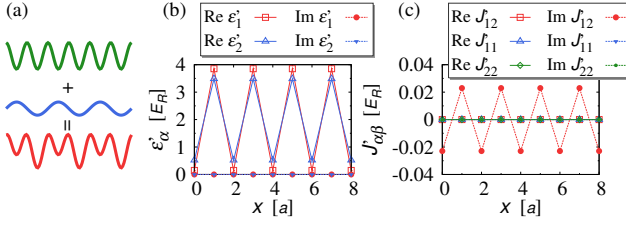


FIG. 1: (a) A schematic diagram of a lattice potential modulation induced by the additional two-site period potential. (b) and (c) The parameters of the additional potential Hamiltonian \mathcal{H}' for $V_0 = 15E_r$ and $V'_0 = 4E_r$. Onsite potential terms $\epsilon'_{i,\alpha}$ are real number, $\text{Im}\epsilon'_{i,\alpha} = 0$. All elements of $J'_{\alpha\beta}$ except for $\text{Im}J'_{12}$ are close to zero.

trapping potential is absent from our model as recently demonstrated in the experiment [15].

In what follows, we define single atoms with $\sigma = \uparrow (\downarrow)$ occupying the lowest orbital $\alpha = 1$ at the i th site as the qubits, and express its state by $|0\rangle_i (|1\rangle_i)$. As we will see later, the other states in the higher orbitals or with multiple occupancies serve as the *controllable and accessible* environment that plays an essential role in our method. It is useful to mention here the general strategy for creating the cluster state $|\text{CS}\rangle$ [2]: first, initialize qubits as the product of superposition states $|+\rangle_i = (|0\rangle_i + |1\rangle_i)/\sqrt{2}$, which are efficiently prepared using the band insulating transition of fermions [16]; then, apply a unitary transformation described by the time evolution with an Ising interaction, namely, $|\text{CS}\rangle = \exp\{-i(\tau/\hbar)J_{\text{Ising}}\sum_i \sigma_i^z \sigma_{i+1}^z\} \prod_i |+\rangle_i$ with the characteristic time $\tau = 4\pi\hbar/J_{\text{Ising}}$. We will show that the unitary transformation can be implemented by simply modulating the optical lattice potentials.

Now, we explain our implementation scheme for realizing the Ising interaction. In addition to the original lattice potential, we apply an extra lattice potential with a two-site period given by $V'_0 \cos(x/2a + \theta)$, where θ is the relative phase between the original and the additional potentials. Here, we chose $\theta = \pi/2$ and set it along the x -direction. Figure 1(a) shows schematically how the combination of these two potentials modifies the lattice landscape. The Hamiltonian originating from this additional potential is written as $\mathcal{H}' = \sum_{i\sigma\alpha} \epsilon'_{i,\alpha} c_{i\sigma\alpha}^\dagger c_{i\sigma\alpha} + \sum_{\langle ij \rangle \sigma \alpha \beta} J'_{i,\alpha\beta} c_{i\sigma\alpha}^\dagger c_{j\sigma\beta}$. We evaluate the parameters $\epsilon'_{i,\alpha}$ and $J'_{i,\alpha\beta}$ with the same *ab initio* calculations as mentioned above. In Fig. 1(b), the on-site potential $\epsilon'_{i,\alpha}$ exhibits staggered modulations as expected from the total potential shape shown in Fig. 1(a). On the other hand, as regards hopping matrices $J'_{i,\alpha\beta}$, we find an interesting and useful feature as shown in Fig. 1(c). Only the inter-orbital J'_{12} has a large magnitude, while the other elements $J'_{i,\alpha\beta}$ are nearly equal to zero. This is because the orthogonality of the Bloch functions is broken by superposing the two-site period potential. In addition, this modulation is commensurate with the original

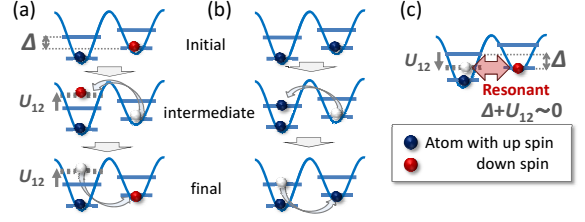


FIG. 2: (a) and (b) Second order virtual hopping processes for two atoms with different and same spins, respectively. Blue solid lines represent the energy levels of the lowest and the second lowest orbitals. The gray dotted line shows the energy shift caused by the interaction. (c) Resonant condition of the Ising interaction with a strength $J_{\text{Ising}} \propto \frac{|J'_{12}|^2}{\Delta + U_{12}} - \frac{|J'_{12}|^2}{\Delta}$.

lattice so that strong inter-orbital coupling is introduced between orbital-1 and 2. Such a striking situation is realized when $\theta = \pi/2 + \ell\pi$ with integer ℓ . As θ deviates from these values, some elements of $J'_{i,\alpha\beta}$ become non-negligible.

Next, we roughly explain the physical mechanism by which the two-site period potential leads to the Ising interaction, based on the second order perturbation theory with specific initial states such as Mott insulators. As is well known, such perturbative processes originating from J_{11} induce Heisenberg type spin interactions with a strength $J_{\text{Heisenberg}} \propto J_{11}^2/U_{11}$. We now consider similar processes in terms of the inter-orbital hopping J'_{12} with a large amplitude. Note that the i -dependence of $J'_{i,12}$ is currently neglected for simplicity. Figure 2(a) and (b) schematically represents the perturbative processes for two localized atoms with different and same spins, respectively. The top panels correspond to the initial Mott states. The middle panels show the virtual intermediate states. It is clear that, for the atoms with different spins, the inter-orbital interaction U_{12} causes the energy shift shown by the gray dotted line, while there is no such energy shift for the atoms with same spins due to the Pauli principle. The bottom panels are the final states, which are exactly the same as the initial states. This is a consequence of an energy conservation law that prohibits spin-exchanging processes with a finite energy difference due to the Bloch bandgap $\Delta = \epsilon_2 - \epsilon_1 + \epsilon'_{i,2} - \epsilon'_{i+1,1}$. Thus, we can conclude that the additional potential results in the Ising interaction with a strength $J_{\text{Ising}} \propto \frac{|J'_{12}|^2}{\Delta + U_{12}} - \frac{|J'_{12}|^2}{\Delta}$ via the perturbation processes.

Here we remark on the controllability of our Ising interaction. We can switch off the interaction at our will by removing the additional lattice potential. More importantly, the interaction strength is increased if the resonant condition $\Delta + U_{12} \sim 0$ is satisfied as shown in Fig. 2(c). We can achieve this resonant condition by controlling $U_{12} (\propto a_S)$ via a Feshbach resonance [17] and also by tuning $\epsilon'_{i,\alpha}$ via the change in V'_0 . The resonant condition of the Ising interaction allows us to reduce the

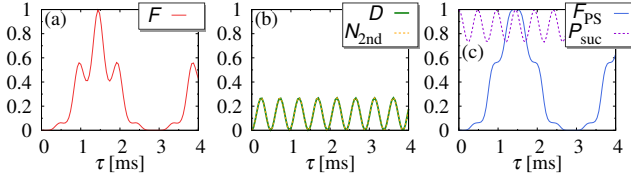


FIG. 3: Simulation results for the 2-qubit system with $V_0 = 10E_r$ and $V'_0 = 6.2E_r$. (a) Fidelity F as a function of time τ . (b) The number of doubly occupied sites D and the atoms with the second lowest orbital N_{2nd} . The two curves overlap each other. (c) Fidelity with the post selection F_{PS} and success probability P_{suc} .

time required for preparing cluster states. Note that the large magnetic interaction is usually difficult to realize via the perturbative mechanism without such a resonance scheme.

The above discussions should be carefully verified by calculating the actual dynamics of atoms without any perturbative approximations. We therefore numerically simulate the time evolution of the present system written as $|\phi(\tau)\rangle = \exp\{i(\tau/\hbar)(\mathcal{H} + \mathcal{H}')\} \prod_i |+\rangle_i$ using an exact diagonalization method. It is found that certain effects not included in the simple second-order perturbation theory degrade both fidelity and scalability of our method. To overcome these problems, we adopt two more strategies in addition to the resonance scheme, namely, *the post-selection scheme* and *the pair-wise scheme*. In the following, we will explain in detail how each scheme of our proposal works well on the basis of numerical simulations.

First of all, we examine our resonance scheme by simulating a 2-qubit system of ^{40}K atoms with the following realistic parameters; $a = 413$ nm, $a_S = -50$ nm, $V_0 = 10E_r$ and $V'_0 = 6.2E_r$, where E_r is the recoil energy. Note that the third lowest and the higher orbitals are negligible because energy levels of them are far off-resonant from that of the lowest orbital. We calculate the fidelity $F \equiv |\langle \text{CS} | \phi(\tau) \rangle|^2$, where $|\text{CS}\rangle$ is equivalent to the Bell pair in 2-qubit entangled states. In Fig. 3(a), the calculated fidelity F is plotted as a function of time τ . A high-fidelity cluster state of $F = 0.997$ is obtained at around 1.5 ms. We thus confirm that our scheme can realize the large Ising interaction enough to generate a cluster state in a short time.

Secondly, we further explore the characteristics of the F curve shown in Fig. 3(a). We can see two types of oscillations with periods of about 3 and 0.5 ms. The longer period oscillation obviously corresponds to the time evolution driven by the Ising interaction. On the other hand, the shorter period oscillation suggests the existence of some additional dynamics during the entanglement generation. To clarify this, we plot in Fig. 3(b) the number of doubly occupied sites D and the number of atoms in the second lowest orbital N_{2nd} as a function of time. Two

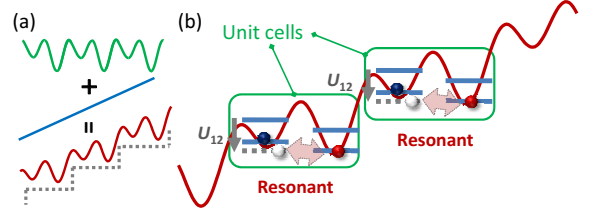


FIG. 4: (a) Overall diagram of a linear potential modulation in addition to the lattice modulation shown in Fig. 1 (a). The dotted line provides a stepwise structure to guide the eyes. (b) A schematic view of the pair-wise scheme, where the Ising interaction is resonantly enhanced only inside the unit cells.

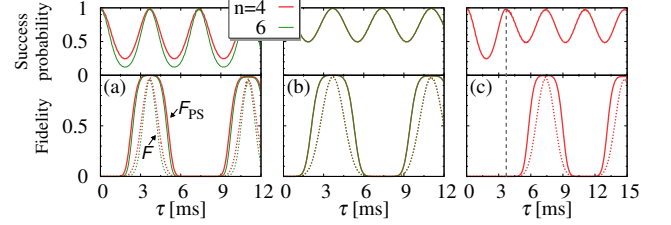


FIG. 5: Simulation results using the pair-wise scheme for 4- and 6-qubit systems with $V_0 = 18E_r$ and $V'_0 = 4E_r$. (a) Fidelity F and F_{PS} , and success probability P_{suc} . (b) Rescaled quantities $F^{2/n}$, $F_{PS}^{2/n}$, and $P_{suc}^{2/n}$, where the curves for different $n = 4$ and 6 overlap each other. (c) Same quantities with the unit cell shift for $n = 4$. The gray dashed line represents the time $\tau = 3.7$ ms at which we move the unit cells.

quantities D and N_{2nd} agree exactly and the oscillation period of them is 0.5 ms. These results mean that the actual excitation of atoms occurs between the 2-qubit state and the intermediate state as depicted in Fig. 2 (a). The shorter period oscillation of F curve is attributed to this excitation. Note that the intermediate state is assumed to be virtual in the simple perturbation theory. The above dynamics beyond this assumption are induced as a trade-off for the large Ising interaction in our resonance scheme.

Here we explain that the fidelity can be enhanced by eliminating the intermediate state via spectroscopic measurements. Specifically, we employ the following post-selection scheme: first, detect D by using, *e.g.*, photo-association spectroscopy [18, 19], or measure N_{2nd} with, *e.g.*, orbital blockade spectroscopy [20]; after that, determine the operation is a success (failure) by the measurement outcome suggesting the absence (existence) of the intermediate states. In Fig. 3(c), we show fidelity with the post selection F_{PS} and the success probability P_{suc} obtained by the same numerical simulation method. As the result of the post selection, the intermediate states are removed, and a shorter period oscillation disappears from the fidelity curve. We can thus achieve an extremely high fidelity of $F_{PS} \sim 1$ in return for the failure probability of $1 - P_{suc} \sim 0.002$.

Thirdly, we simulate n -qubit systems for $n > 2$ so as

to discuss scalability. When we apply our scheme to 4-qubit system in a similar way to that described above, we obtain the fidelity of $F_{\text{PS}} \sim 0.71$ with $P_{\text{suc}} \sim 0.931$. This crucial decrease in the fidelity is attributed to extra excitation processes that are not included in those shown in Fig. 2(a) and (b). For instance, in the intermediate state shown in Fig. 2(a), the excited atom does not always go back to the initial site, but instead further moves to the third lattice site. Such extra excitations may occur except in 2-qubit systems.

To suppress the extra excitations, we divide the system into a set of effective 2-qubit systems, and then independently generate an entanglement in each 2-qubit system. We realize this pair-wise scheme by adding a linear potential gx with a gradient g as demonstrated in the experiment [21]. Figure 4(a) schematically represents the linear potential modulation. Here we find a characteristic stepwise structure. As shown in Fig. 4(b), we define each step consisting of two lattice sites as a unit cell, and properly tune the resonant condition $\Delta + U_{12} \sim 0$ satisfied only inside the unit cells. Consequently, the Ising interaction is made pair-wise, and thus entanglement of two qubits in each unit cell can be generated simultaneously and separately.

Using the pair-wise scheme mentioned above, we perform numerical simulations for $n > 2$, and again discuss scalability. Here, we calculate the fidelity F between a product state of Bell pairs in unit cells and $|\phi(\tau)\rangle$. In Fig. 5(a), we show results for $n = 4$ and 6 with $V_0 = 18E_r$ and $V'_0 = 4E_r$. High fidelity cluster states for $n = 4(6)$ are generated with or without the post selection as $F_{\text{PS}} \sim 0.999(0.998)$ with $P_{\text{suc}} \sim 0.987(0.980)$ or $F \sim 0.973(0.960)$, respectively. With the ideal pair-wise scheme, all of these quantities should be scaled as, *e.g.*, $F = \tilde{F}^{n/2}$ where the tilde represents quantities per unit cell. In Fig. 5(b), we show rescaled quantities $F^{2/n}$, $F_{\text{PS}}^{2/n}$ and $P_{\text{suc}}^{2/n}$. For all of these quantities, the rescaled curves for $n = 4$ and 6 overlap each other, suggesting that the Ising interaction is almost perfectly pair-wise. Here we have obtained the unit cell fidelity of $\tilde{F}_{\text{PS}} \sim 0.999$ with $\tilde{P}_{\text{suc}} \sim 0.993$ or $\tilde{F} \sim 0.987$. These values reflect that our pair-wise scheme strongly suppresses the extra excitations.

We further extend our scheme for generating multipartite entangled states over whole 1D lattice sites. After the set of Bell pairs are prepared as mentioned above, we move unit cells toward one site right or left by changing the sign g or the relative phase $\theta = \pi/2 \rightarrow 3\pi/2$, and then again perform pair-wise entanglement generation. In Fig. 5(c), we show simulation results for $n = 4$ with the same parameters as above, where unit cells are shifted at time $\tau = 3.7$ ms indicated by the gray dashed line. By combining our several techniques, we finally obtain very high-fidelity cluster states, $F_{\text{PS}} = 0.998(\sim \tilde{F}_{\text{PS}}^3)$ with $P_{\text{suc}} = 0.979(\sim \tilde{P}_{\text{suc}}^3)$ or $F \sim 0.961(\sim \tilde{F}^3)$. An

important point of this result is that we succeed in suppressing the effects of uncommutative interactions, such as the Heisenberg interaction. Namely, we can set $J_{\text{Ising}} \gg J_{\text{Heisenberg}}$ in our scheme.

Finally, we discuss the generation of 2D and 3D cluster states. So far, we have discussed the 1D entanglement generation, where the inter-orbital hopping J'_{12} with a large magnitude is only induced along the x -direction. Importantly, this directivity helps us to suppress the extra excitation processes along the y - and z -directions. Thanks to the directivity and commutativity of our Ising interaction, the successive 1D entanglement generation by changing the direction allows us to generate 2D and 3D cluster states, which will be useful for fault tolerant MBQC [11–13]. Note that the failure event of the post selection can be regarded as loss of qubits. Therefore, our scheme, which enhances the fidelity in return for the increased losses, is suitable for the fault tolerant MBQC that is robust against losses [14].

In summary, we propose a method for controlling the quantum state of ultracold atoms in an optical lattice. Utilizing higher Wannier orbital states, we realize a tunable pair-wise Ising interaction between atoms in the lowest orbital. This scheme can generate high-fidelity entangled cluster states, which is useful for scalable MBQC. As a prospect, we note that our tunable magnetic interaction can be employed for quantum simulations of magnetism, for instance, demonstration of the Néel transition. We also remark that our basic concept, Wannier orbital controlling, can be realized in both fermionic and bosonic systems. Finally, we expect that our scheme is not limited to only these applications, but will also find a wide range of uses with respect to quantum state manipulations and quantum information processing.

We thank Y. Takahashi, K. Azuma, Y. Matsuzaki, and Y. Tokura for valuable discussions.

-
- [1] H. J. Briegel, D. E. Browne, W. Dur, R. Raussendorf, and M. Van den Nest, *Nat. Phys.* **5**, 19 (2009).
 - [2] R. Raussendorf and H. J. Briegel, *Phys. Rev. Lett.* **86**, 5188 (2001).
 - [3] I. Bloch, *Nature (London)* **453**, 1016 (2008).
 - [4] W. S. Bakr, A. Peng, M. E. Tai, R. Ma, J. Simon, J. I. Gillen, S. Fölling, L. Pollet, and M. Greiner, *Science* **329**, 547 (2010).
 - [5] C. Weitenberg, M. Endres, J. F. Sherson, M. Cheneau, P. Schauß, T. Fukuhara, I. Bloch, and S. Kuhr, *Nature (London)* **471**, 319 (2011).
 - [6] L.-M. Duan, E. Demler, and M. D. Lukin, *Phys. Rev. Lett.* **91**, 090402 (2003).
 - [7] O. Mandel, M. Greiner, A. Widera, T. Rom, T. W. Hansch, and I. Bloch, *Phys. Rev. Lett.* **91**, 010407 (2003).
 - [8] B. Vaucher, A. Nunnenkamp, and D. Jaksch, *New J. Phys.* **10**, 023005 (2008).
 - [9] L. Jiang, A. M. Rey, O. Romero-Isart, J. J. Garcia-Ripoll,

- A. Sanpera, and M. D. Lukin, Phys. Rev. A **79**, 022309 (2009).
- [10] O. Mandel, M. Greiner, A. Widera, T. Rom, T. W. Hänsch, and I. Bloch, Nature (London) **425**, 937 (2003).
- [11] R. Raussendorf, J. Harrington, and K. Goyal, Ann. Phys. (NY) **321**, 2242 (2005).
- [12] R. Raussendorf, J. Harrington, and K. Goyal, New J. Phys. **9**, 199 (2007).
- [13] R. Raussendorf and J. Harrington, Phys. Rev. Lett. **98**, 190504 (2007).
- [14] T. M. Stace, S. D. Barrett, and A. C. Doherty, Phys. Rev. Lett. **102**, 200501 (2009).
- [15] S. Will, T. Best, U. Schneider, L. Hackermüller, D.-S. Luhmann, and I. Bloch, Nature (London) **465**, 197 (2010).
- [16] M. Köhl, H. Moritz, T. Stöferle, K. Günter, and T. Esslinger, Phys. Rev. Lett. **94**, 080403 (2005).
- [17] C. A. Regal and D. S. Jin, Phys. Rev. Lett. **90**, 230404 (2003).
- [18] T. Rom, T. Best, O. Mandel, A. Widera, M. Greiner, T. W. Hänsch, and I. Bloch, Phys. Rev. Lett. **93**, 073002 (2004).
- [19] S. Sugawa, K. Inaba, S. Taie, R. Yamazaki, M. Yamashita, and Y. Takahashi, Nat. Phys. **7**, 642 (2011).
- [20] W. S. Bakr, P. M. Preiss, M. E. Tai, R. Ma, J. Simon, and M. Greiner, Nature (London) **480**, 500 (2011).
- [21] J. Simon, W. S. Bakr, R. Ma, M. E. Tai, P. M. Preiss, and M. Greiner, Nature (London) **472**, 307 (2011).